

The wall shear rate distribution for flow in random sphere packings

Patrick B. Warren¹ and Frantisek Stepanek²

¹*Unilever R&D Port Sunlight, Bebington, Wirral, CH63 3JW, UK.*

²*Chemical Engineering and Chemical Technology, Imperial College, London, SW7 2AZ, UK.*

(Dated: October 22nd, 2007 — revised submission of LF11477 Warren)

The wall shear rate distribution $P(\gamma)$ is investigated for pressure-driven Stokes flow through random arrangements of spheres at packing fractions $0.1 \leq \phi \leq 0.64$. For dense packings, $P(\gamma)$ is monotonic and approximately exponential. As $\phi \rightarrow 0.1$, $P(\gamma)$ picks up additional structure which corresponds to the flow around isolated spheres, for which an exact result can be obtained. A simple expression for the mean wall shear rate is presented, based on a force-balance argument.

PACS numbers: 47.56.+r, 47.15.G-

The wall shear rate γ is the rate at which the tangential velocity of a fluid vanishes on approaching a wall. It determines the hydrodynamic forces acting on a particle adjacent to the wall, and is therefore a key quantity governing deposition, retention, and detachment [1]. For example, γ is an important factor which determines whether colloidal particles can become attached to a surface by specific ligand binding [2]. Experimentally, such processes are often examined using flow cells with well-controlled hydrodynamics for which the wall shear rate is known. For flow through a porous material though, one can expect a *distribution* of wall shear rates $P(\gamma)$. This is illustrated in Fig. 1. A crucial issue for realistic situations, such as deep bed filtration [3] or particulate soil detergency in fabric cleaning [4], is therefore to characterise the wall shear rate distribution $P(\gamma)$ for flow in more complex pore spaces. This is also a problem of generic interest in the growing field of statistical microhydrodynamics. Previously, only $P(\gamma)$ for flow in two-dimensional channels with (fractally) rough walls has been investigated [5].

In this Letter, $P(\gamma)$ and its relation to the mean fluid velocity U_m is investigated for pressure-driven Stokes flow in random sphere packings at packing fractions in the range $0.1 \leq \phi \leq 0.64$. The relationship between $P(\gamma)$ and U_m is of paramount importance for applications since it is very difficult to access $P(\gamma)$ experimentally (it either has to be done by detailed resolution of the flow field, or indirectly by looking at the behaviour of particulate tracers), but determination of U_m is much easier.

We generated sphere packings in periodic simulation boxes for packing fractions in the range $0.1 \leq \phi \leq 0.64$ by a Monte-Carlo algorithm [6]. The highest packing fraction corresponds to the usual random close-packed limit. Whilst the lower packing fractions are mechanically unstable, they provide a useful interpolation between isolated spheres and packed beds. We also generated a slightly looser packing of touching spheres at $\phi \approx 0.622$ by a sequential deposition algorithm [7]. This latter geometry is not periodic in the z -direction (the deposition direction), but we have found that the bulk properties can be determined by extrapolation.

For the flow-field calculations we use a standard lattice Boltzmann (LB) methodology which is now well-developed for this class of problems [8, 9, 10, 11, 12, 13, 14, 15]. As already mentioned, we solve the Stokes equations and thus operate at strictly zero Reynolds number. The spheres are held stationary and flow is generated in the pore space by applying a uniform body force corresponding to a mean pressure gradient $(\nabla p)_m$ in the x -, y - or z -directions. The hydrodynamic forces exerted on wall lattice nodes are easily found in LB. For each wall node one can trivially determine the tangential force component since the corresponding sphere centre is known. The local wall shear rate is then given by the magnitude of the tangential component divided by the viscosity. In this way we obtain a large set of wall shear rates from which we reconstruct $P(\gamma)$ [16]. We also measure the mean volumetric (superficial) fluid velocity U_m .

We first discuss our results for the permeability, k , since this underpins our analysis of $P(\gamma)$. It is defined via Darcy's law, $U_m = (k/\eta)(\nabla p)_m$, where η is the viscosity. Our results, expressed in dimensionless terms using k/σ^2 , are shown as a function of packing fraction in Table I and Fig. 2. Generally speaking, the permeability falls dramatically with increasing packing fraction. For $\phi \leq 0.5$ our results are in excellent agreement with previous work by Ladd [17] and van der Hoef *et al.* [13]. For $\phi \geq 0.6$ our results are $\approx 10\%$ higher than the accurate results obtained recently by van der Hoef *et al.* [13], although we are in agreement with some previous studies [9, 18]. This may reflect subtle differences in the way the sphere packings are constructed. The sequential deposition packing at $\phi \approx 0.622$ fits nicely into the series. In this case the permeability is in principle different parallel to and perpendicular to the deposition direction. We find though that the difference is certainly less than 10%, in agreement with Coelho *et al.* [7].

An oft-used correlation is the Kozeny-Carman relation,

$$k = (1 - \phi)^3 / c_0 s^2, \quad (1)$$

where $s = 6\phi/\sigma$ is the specific surface area of spheres (in any arrangement) and the numerical factor $c_0 \approx 4-5$ [9, 12, 18, 19]. We find this does indeed capture the

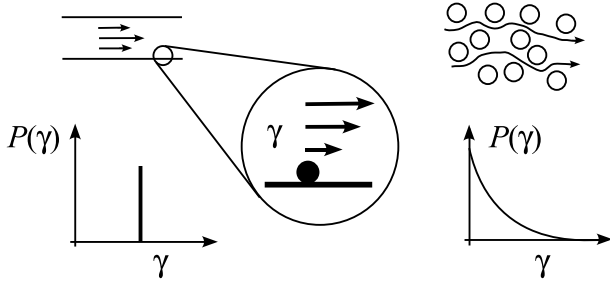


FIG. 1: The flow in the controlled geometry of a flow cell gives rise to a uniform wall shear rate (left), whereas the flow in a porous material gives rise to a *distribution* of wall shear rates (right). It is the wall shear rate γ that governs the deposition and detachment of particles (inset).

behaviour of the permeability quite well for intermediate to high packing fractions (Table I). Interestingly, for $\phi \geq 0.2$ we noticed our data can be accurately fit by $\log(k/\sigma^2) = A + B\phi$ with $A = -1.04(6)$ and $B = -9.6(1)$, reminiscent of what has been found for fibrous beds [10].

Now we turn to the mean wall shear rate, defined via $\gamma_m = \int_0^\infty d\gamma \gamma P(\gamma)$. For Stokes flow, γ_m is strictly proportional to U_m , so that $\sigma\gamma_m/U_m$ is a convenient way to express the mean wall shear rate in dimensionless terms, shown in Table I and Fig. 2. We see that $\sigma\gamma_m/U_m$ grows dramatically with packing fraction, similar to the inverse of k/σ^2 .

This behaviour can be understood by the following force-balance argument. The force per unit volume acting on the fluid due to the mean pressure gradient is $(1 - \phi)(\nabla p)_m$. In steady state this must balance the integrated wall stress, thus the mean wall stress is *exactly* $(1 - \phi)(\nabla p)_m/s$ where s is the specific surface area. If we now *approximate* the mean wall stress by $\eta\gamma_m$, use Darcy's law to replace $(\nabla p)_m$ by U_m , and substitute $s = 6\phi/\sigma$, we get

$$\gamma_m = \alpha(1 - \phi)\sigma U_m / (6\phi k). \quad (2)$$

We have introduced a prefactor α to capture the approximate nature of this expression. From our data we find that $\alpha \approx 0.6$ – 0.8 is very insensitive to packing fraction, as shown in Table I (we can rationalise this value of α by arguing that, on average, $2/3$ of the wall stress lies in the wall tangent plane). Eq. (2) explains the approximate inverse relationship between $\sigma\gamma_m/U_m$ and k/σ^2 . Incidentally, in a parallel-sided capillary of arbitrary cross section, the flow is laminar and parallel to the walls. In this case the mean wall stress is exactly $\eta\gamma_m$ and Eq. (2) is exact with $\alpha \equiv 1$. Our LB methodology is constructed to retain this exact result, provided the capillary axis is aligned with a grid axis.

Finally we turn to the wall shear rate distribution, which we report in terms of $x = \gamma/\gamma_m$ and $f(x)$ defined such that $P(\gamma) = (1/\gamma_m) f(\gamma/\gamma_m)$. At packing fractions $\phi \geq 0.6$, $f(x)$ is monotonic and quite well approximated

ϕ	$k/\sigma^2 \times 10^3$	c_0	$\sigma\gamma_m/U_m$	α
0.1	203(8)	10.0(4)	4.4(2)	0.60(2)
0.2	53(2)	6.7(3)	7.6(3)	0.60(2)
0.4	7.4(3)	5.1(2)	21.1(5)	0.62(3)
0.5	2.9(1)	4.8(2)	37(1)	0.64(2)
0.6	1.09(6)	4.5(2)	69(2)	0.68(4)
0.622 (<i>z</i>)	0.97(7)	4.0(3)	81(7)	0.78(6)
0.622 (<i>xy</i>)	0.89(6)	4.4(3)	78(6)	0.69(5)
0.64	0.74(4)	4.3(2)	92(4)	0.73(4)

TABLE I: Dimensionless permeability k/σ^2 and mean wall shear rate $\sigma\gamma_m/U_m$ as a function of packing fraction ϕ : c_0 is the Kozeny-Carman factor in Eq. (1) and α is the prefactor in the force-balance expression in Eq. (2). For the sequential deposition sample ($\phi \approx 0.622$), results are given parallel and perpendicular to the deposition direction (*z*). A figure in brackets is an estimate of the error in the final digit [15].

by an exponential (Fig. 3, upper plot). It is interesting to note that a similar exponential distribution is found for the local flow speeds although in this case a peak at zero is to be expected given the large volume of pore space immediately adjacent to the sphere surfaces [11, 12]. We will return to the small x behaviour of $f(x)$ in a moment.

As the packing fraction is reduced, a hump appears in $f(x)$ at around $x = 0.5$ – 0.6 (Fig. 3, lower plot). This feature seems to be associated with the transition from channel flow at high packing fractions towards flow around individual spheres at lower packing fractions. This interpretation is supported by the exact result which can be obtained for $P(\gamma)$ from the Stokes solution for flow around a sphere, as we now discuss.

A remarkable feature of Stokes flow around a sphere is that the wall stress has the same vectorial value $3\eta\mathbf{U}/\sigma$ at all points on the sphere surface, where \mathbf{U} is the flow velocity at infinity [20]. If we project this into the wall tangent plane, we obtain the local wall shear rate $\gamma = (3U_m \sin \theta)/\sigma$, where θ is the angle between the wall normal and the direction of the flow field at infinity, and $U_m \equiv |\mathbf{U}|$. The mean wall shear rate is then given by $\sigma\gamma_m/U_m = \int_0^\pi (3/2) \sin^2 \theta d\theta = 3\pi/4 \approx 2.356$. It follows that $x = \gamma/\gamma_m = (4/\pi) \sin \theta$, and from $f(x) dx = (1/2) \sin \theta d\theta$ (*i. e.* the area measure [16]),

$$f(x) = \frac{\pi x/4}{\sqrt{(4/\pi)^2 - x^2}}, \quad 0 \leq x \leq 4/\pi. \quad (3)$$

This is the desired exact result for the wall shear rate distribution for Stokes flow around an isolated sphere, shown as the dotted line in the lower plot of Fig. 3. It diverges as $x \rightarrow 4/\pi \approx 1.273$, corresponding to $\theta \rightarrow \pi/2$ where the wall shear rate is maximal. This behaviour is, we believe, responsible for the hump that appears in $f(x)$ at low packing fractions. The fact that there is still a significant difference between Eq. (3) and $f(x)$

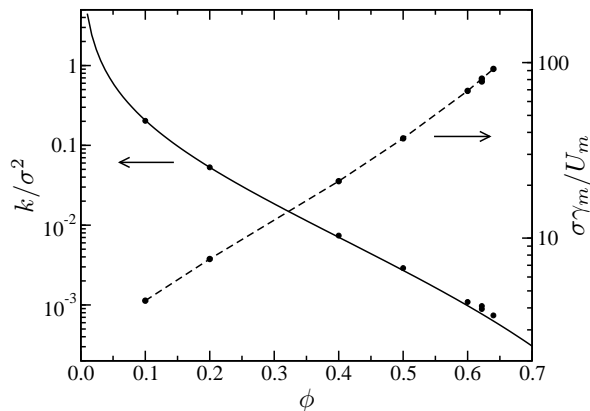


FIG. 2: Dimensionless permeability and mean wall shear rate as a function of packing fraction, from Table I. The solid line is Eq. (31) from van der Hoef *et al.* [13] which is claimed to be accurate to within 3%. The dashed line for the mean wall shear rate data is a guide to the eye. Error bars are smaller than the symbols.

for $\phi = 0.1$ should not be too surprising given the long range nature of hydrodynamic interactions. We see this also in k and γ_m which are, respectively, a factor ≈ 2.76 smaller and a factor ≈ 1.9 higher, than the corresponding isolated sphere limits (*i.e.* $k/\sigma^2 = 1/(18\phi)$ [17, 21] and $\sigma\gamma_m/U_m = 3\pi/4$ derived above). In fact the permeability data from Ladd suggests that the isolated sphere result is approached only very slowly as $\phi \rightarrow 0$ [17].

Now we return to the small x behaviour of $f(x)$. Clearly, for any sphere, the local wall shear rate has to vanish at least at one point on the sphere surface—this is a consequence of the so-called ‘hairy ball theorem’ [22]. Thus it is not at first sight surprising that $f(x)$ goes to a plateau as $x \rightarrow 0$ (Fig. 3, lower plot). However, Eq. (3) has the property that $f(x) \sim x$ as $x \rightarrow 0$ arising from the stagnation points at $\theta = (0, \pi)$. This behaviour might be expected to be generic for low packing fractions where stagnation points are common. In contrast, for dense sphere packings the flow is more channel-like and stagnation points are rare. In this case the wall shear rate vanishes, *inter alia*, at all the contact points between spheres. Analysis of pressure-driven flow in the vicinity of a contact point using the Reynolds lubrication equation [23] suggests $f(x) \sim x^\delta$ for $x \rightarrow 0$ where $\delta = (4 - \sqrt{10})/(\sqrt{10} - 2) \approx 0.72$. It is therefore rather surprising that, independent of packing fraction, a *plateau* rather than a power law is observed for $f(x)$ as $x \rightarrow 0$.

One possible reason for this is that long-range flow field inhomogeneities (on length scales $\gtrsim \sigma$) wash out the expected behaviour and replace the power law by a plateau. We investigated this possibility by constructing an individual $f(x)$ for each sphere, then averaging over all the spheres in a sample. This should remove the effects of long-range flow field inhomogeneities. We find though

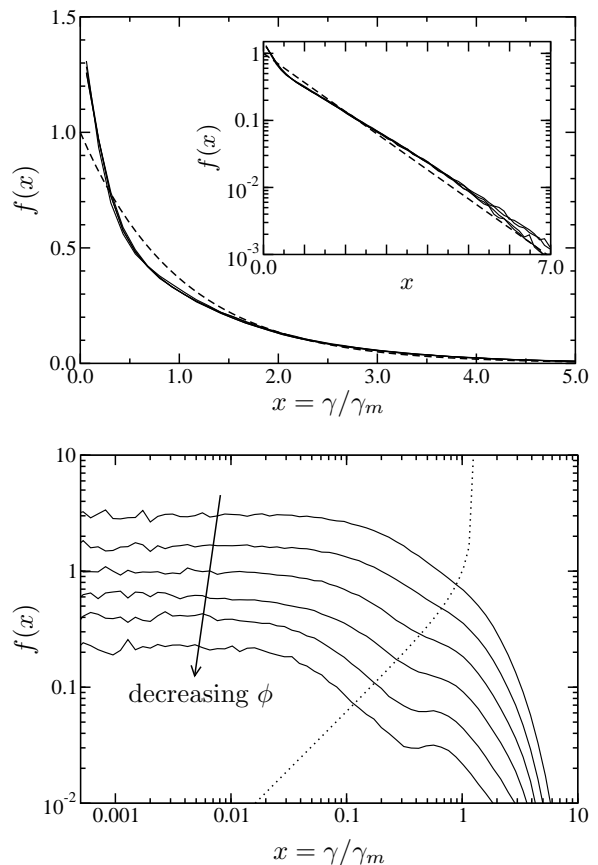


FIG. 3: The upper plot shows the wall shear rate distributions for all data sets with $\phi \geq 0.6$. The dashed line is $f(x) = e^{-x}$. The lower plot shows the same for the six periodic packings with $0.1 \leq \phi \leq 0.64$; the curves are displaced for clarity. The dotted line is the exact result in Eq. (3) for Stokes flow around an isolated sphere.

there is little change in $f(x)$; the hump at low ϕ becomes somewhat more pronounced but the plateau remains in all cases. At the same time we also examined the hydrodynamic forces acting on individual spheres. We found that these have a relatively narrow distribution (approximately Gaussian, with a standard deviation 20–30% of the mean) indicating that the flow field on length scales $\gtrsim \sigma$ is rather homogeneous. We conclude that long-range flow field inhomogeneities are unlikely to be important. Instead, the implication is that the shape of $f(x)$, and in particular the plateau at $x \rightarrow 0$, is mostly controlled by the local pore geometry. The important message seems to be that using highly idealised situations, such as the Stokes solution for flow around an isolated sphere or lubrication theory in the vicinity of a contact point, may give qualitatively misleading results when it comes to inferring the overall statistical properties.

To summarise, for applications Eq. (2) provides the key link between the mean wall shear rate γ_m and the mean fluid velocity U_m . If necessary the Darcy permeability can be estimated from the Kozeny-Carman

relation in Eq. (1). Knowledge of γ_m is then sufficient to determine the whole wall shear rate distribution, if the latter is assumed to be exponential, *i. e.* $P(\gamma) \approx (1/\gamma_m) \exp(-\gamma/\gamma_m)$. More generally, our investigation demonstrates how direct numerical calculation of the statistical properties of microhydrodynamic flows can complement exact solutions for simplified geometries, to gain new insights.

We thank Theo van de Ven for helpful discussions, and the Unilever Centre for Molecular Science Informatics in the University of Cambridge for access to the computational resources of the ‘CamGrid’ network.

-
- [1] T. G. M. van de Ven, *Colloidal Hydrodynamics* (Academic, San Diego, 1989).
 - [2] See for example K.-C. Chang, F. J. Tees, and D. A. Hammer, *Proc. Natl. Acad. Sci. USA* **97**, 11262 (2000); G. Pangu *et al.*, *Langmuir* **23**, 10682 (2007).
 - [3] See for example T. G. M. van de Ven, *Coll. Surf. A* **138**, 207 (1998); N. P. Ryde and E. Matijević, *Coll. Surf. A* **165**, 59 (2000).
 - [4] See for example E. Kissa, *Textile Res. J.* **48**, 395 (1978); B. J. Carroll, *Coll. Surf. A* **74**, 131 (1993).
 - [5] J. S. Andrade, Jr. *et al.*, *Phys. Rev. Lett.* **98**, 194101 (2007).
 - [6] F. Stepanek, A. Loo, and T. S. Lim, *J. Pharm. Sci.* **95**, 1614 (2006).
 - [7] D. Coelho, J.-F. Thovet, and P. M. Adler, *Phys. Rev. E* **55**, 1959 (1997).
 - [8] A. J. C. Ladd, *J. Fluid Mech.* **271**, 285; 311 (1994).
 - [9] A. W. J. Heijs and C. P. Lowe, *Phys. Rev. E* **51**, 4346 (1995).
 - [10] A. Koponen *et al.*, *Phys. Rev. Lett.* **80**, 716 (1998).
 - [11] C. Manwart *et al.*, *Phys. Rev. E* **66**, 016702 (2002).
 - [12] R. S. Maier *et al.*, *J. Coll. Int. Sci.* **217**, 341 (1999).
 - [13] M. A. van der Hoef, R. Beetstra, and J. A. M. Kuipers, *J. Fluid Mech.* **528**, 233 (2005).
 - [14] C. Pan, L.-S. Luo, and C. T. Miller, *Computers & Fluids* **35**, 898 (2006).
 - [15] We use a 15-velocity LB scheme with link-bounce-back, similar to that developed by Ladd [8]. To reduce discretisation errors we use a grid refinement procedure similar to van der Hoef *et al.* [13]. Typically 5 sphere packings of size $(5\sigma)^3$ times 3 flow directions were used for each ϕ . The errors arising from sample averaging and grid refinement are estimated to be both of the order 2–3%.
 - [16] An area measure is used in computing the statistical properties, in other words, equal weights are assigned to equal wall areas. This is by no means the only measure that could be contemplated, although we leave exploration of this aspect to future work.
 - [17] A. J. C. Ladd, *J. Chem. Phys.* **93**, 3484 (1990).
 - [18] D. M. E. Thies-Weesie and A. P. Philipse, *J. Coll. Int. Sci.* **162**, 470 (1994).
 - [19] P. C. Carman, *Trans. Inst. Chem. Eng.* **15**, 1550 (1937).
 - [20] G. K. Batchelor, *Fluid Dynamics* (CUP, Cambridge, 1967).
 - [21] N. S. Martys, S. Torquato, and D. P. Bentz, *Phys. Rev. E* **50**, 403 (1994).
 - [22] *I. e.* a hairy ball cannot be combed flat, see for example M. Eisenberg and R. Guy, *Am. Math. Monthly* **86**, 572 (1979); the original proof is H. Poincaré, *J. Math. Pures Appl. (4)* **1**, 167 (1885).
 - [23] A. Oron, S. H. Davis, and S. G. Bankhoff, *Rev. Mod. Phys.* **69**, 931 (1997).